# Experimental Stark widths and shifts and transition probabilities of several Xe II lines

M. A. Gigosos, S. Mar, C. Pérez, and I. de la Rosa
*Departamento de Optica, Universidad de Valladolid, 47071 Valladolid, Spain*
(Received 12 May 1993; revised manuscript received 24 August 1993)

This work reports measured Stark widths and shifts, and transition probabilities for a large number of Xe II spectral lines. A pulsed arc was used as a plasma source. The electron density, determined by interferometry at one wavelength, and simultaneously by the Stark broadening of the 5016-Å He I line, covers a range of $(0.2\text{–}1.8)\times10^{23}\,\mathrm{m}^{-3}$. A method is proposed to find simultaneously the plasma temperature and the transition probabilities from relative intensity measurements of spectral lines. Electron temperatures are in the range of 11 000–16 000 K. The measured parameters are compared with experimental data taken from the literature.

PACS number(s): 52.70.Kz, 32.60.+i

## I. INTRODUCTION

There are a number of important publications in the literature containing Stark broadening parameters of atoms and ions of inert gases. In particular, data referring to Xe II lines appear in Refs. [1–9]. The application in collision physics, photoelectronics, spectroscopy, plasma disgnostics, etc. in xenon present the need to have reliable data of transition probabilities and lifetime. The data from the work cited herein present a dispersion which invites new experimental measurements to be made. The determination of transition probabilities from the intensities of the spectral lines demands an accurate determination of the source characteristics, in particular, the population of the emitting species and the plasma temperature, as well as an absolute calibration of the system. These methods mean the use of expensive, complicated, and sometimes imprecise techniques.

In this work, we have obtained Stark broadening parameters of an important number of Xe II lines; for some of them no prior experimental results exist. These Xe II linewidth and shift measurements contribute an additional set of reliable data in order to determine the atomic parameters which describe Stark broadening phenomena. Undoubtedly, this paper provides an important set of very accurate data.

A reliable study of the Stark broadening of spectral lines requires independent determinations of electron density, plasma temperature, and line shape profiles. Only in this way is it possible to be sure about the accuracy of the measurements before making any comparison with other experimental data. This is exactly what has been done in the present work. As will be described in the following paragraphs, in this experiment the electron density was carefully determined from interferometry, which is independent from Stark broadening, and by the width of the 5016-Å line of He I, calibrated in a previous work [10].

In this work a method is proposed which allows us to obtain simultaneously the plasma temperature and the transition probabilities of the lines studied, exclusively from the relative intensities of spectral lines. The procedure is based on an adequate statistical treatment of the experimental data which requires a great number of spectral lines, in varying plasma conditions, to be measured. The absolute values of the transition probabilities are obtained by comparison with the data from other works.

It is important that the spectroscopic measurements are accurate, i.e., they should have a sufficient spectral resolution and a controllable self-absoption. A knowledge of broadening mechanisms other than the Stark mechanism is also desirable.

## II. EXPERIMENTAL ARRANGEMENT AND PROCEDURE

All measurements have been made in a pulsed discharge. The experimental setup (shown in Fig. 1) and the methods have already been described [11, 12]. Here we will add some more details concerning the present experiment, and the principles of the apparatus will be summarized.

The source of plasma basically consists of a cylindrical

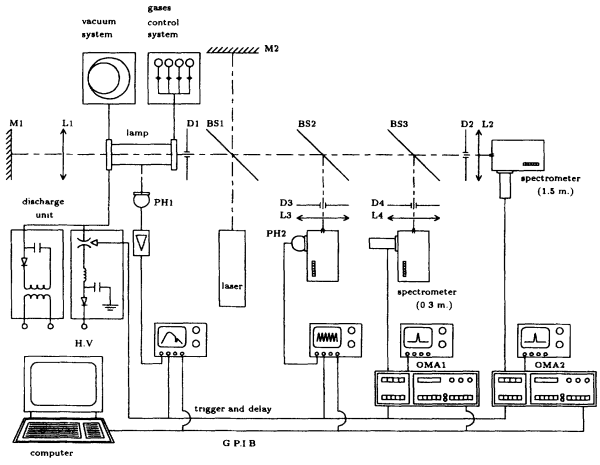


FIG. 1. Experimental setup. GPIB denotes a general-purpose interface bus.

 

tube of Pyrex glass, 155 mm long and 20 mm in interior diameter. Different electrode designs were tried in order to reduce sputtering and to eliminate as much as possible the layers of cold plasma adjacent to the windows. The option chosen consists in placing the electrodes, made of aluminium, in such a way that the glass tube projected farther than the electrode. Thus the electrode was hidden from the discharge. Futhermore, the window was separated 10 mm from the electrode by means of a metal ring electrically isolated from the electrode. With this, the interior separation between windows was 175 mm. This design allowed more than 2500 discharges to be performed without the windows being damaged. The electric connections to the electrodes were made using four rigid rods on each electrode, parallel to the axis of the lamp and symmetrically distributed around it so as to avoid nonhomogeneity in the plasma during the discharge [11].

First we preionized the gas with a continuous current of serveral mA in order to ensure the best conditions for plasma repetitiveness. Afterwards, the plasmas were created by discharging a capacitor bank of 20 $\mu$F charged up to 9 kV. These condensers are connected to one another and to the discharge system by self-inductions which reduce the temporal derivative of the intensity of the current to obtain the best line profiles [11]. On the average, our plasmas lasted for 350 $\mu$s.

During the whole experiment the lamp was working with a continuous flow of helium gas at a rate of 65 $cm^3$/min, and a pressure of 30 mbar. Small quantities of xenon were added to the carrying gas. The amount of xenon was chosen in order to give good intensities to the spectral lines and at the same time to ensure minimal self-absorption.

Spectroscopic and interferometric measurements have been made simultaneously throughout the plasma life. The plasma is viewed end-on through the lamp windows. According to Fig. 1, the discharge lamp is placed in one of the arms of a Twyman-Green interferometer illuminated with a He-Ne laser (6328 Å). At the exit arm of the interferometer, a beam splitter (BS2) splits the light into two beams, which are directed to the spectroscopic and the interferometric channels, respectively. The latter is focused onto the entrance slit of a monochromator which is tuned to the He-Ne laser wavelength. At the exit slit the light is detected by the photomultiplier (PH2), and then it is sent to a digital oscilloscope and transferred to the computer for data analysis. The sample rate of these measurements is 50 ns.

The other beam is divided again by another beam splitter (BS3). Two spectrometers were used for the plasma light studies. A Jarrell-Ash (0.3 m) spectrometer equipped with an optical multichannel analyzer (OMA1) was used to monitor the He I 5016-Å line in order to control the plasma repetitiveness, which was found to be very good, with very small variations. This OMA1 has a vidicon which is divided into 500 channels. The dispersion was 1.2670 Å/channel at 5852 Å. The second spectrometer, a Jobin-Yvon (1.5 m) with a 1200 lines/mm holographic grating, equipped with another optical multichannel analyzed (OMA2), was used for line profile and line shift measurements. The OMA2 has a detector array which is divided into 512 channels. The dispersion was 0.1259 Å/channel at 5890 Å in the first order of diffraction and 0.0459 Å/channel at the same wavelength and in the second order of diffraction.

Care was taken to investigate the possible influence of self-absorption effects on the line profiles, the lens L1 and the flat mirror M1 placed behind the plasma column serve to measure the optical depths of the plasma for each line. This lens forms the image of the lamp center onto itself, and to avoid any modification of the beam collimation in the interferometric arrangement, it is necessary that the lens focus lies on the flat mirror.

The OMA2 has a very important role in the detecting system and therefore it was very carefully calibrated in wavelength as well as in intensity [13]. Wavelength calibration was obtained using spectra of very narrow lines, emitted from different spectral lamps. Intensity calibration was done with the help of an incandescent calibrated lamp, which emitted as a blackbody at 3014.1 K. This calibrated lamp was placed in the experimental setup in the same position as the discharge lamp in order to ensure the same state of polarization for the light reaching the detecting system. The determination of the temperature by means of the relative intensities of the spectral lines was made only with the spectra obtained at the first order of diffraction so as to avoid the indetermination in the calibration process of the second order, the product of the superposition of orders.

The operation process of the two multichannel detectors and the oscilloscope measuring the photomultiplier PH2 was controlled by the computer and activated by the experiment itself. The synchronization of the detecting system with the rest of the experiment was achieved by triggering the whole experiment by the OMA2. The light from the lamp, recorded by the photomultiplier PH1, was monitored together with the pulse of the OMA2 just to be sure that all the spectra were taken at the right moment and with the appropriate pulse width.

The OMA2 was pulsed for 10 $\mu s$. This small pulse width was taken in order to have an acceptable signal-to-noise ratio, a sufficient time resolution, and to be able to follow the temporal plasma evolution.

The experiment consists of successive discharges. On each discharge the following are recorded and stored in the computer: (a) an interferogram which accounts for the complete temporal evolution of the refractivity of the plasma from which we obtain the electron density in each temporal instant, (b) a high-resolution spectrum of the line studied in a predetermined instant in the life of the plasma, (c) a low resolution spectrum of the 5016-Å line of He I in the same instant as the previous one, (d) the complete temporal evolution of the luminous signal of the plasma, and (e) a replica of the trigger pulses of the plasma and of the obturation of the detectors.

The successive discharges are organized in such a way as to obtain (a) temporal evolution of each of the lines studied and (b) control of the self-absorption of the lines through measurements, in identical conditions, with and without the mirror M1 (see Fig. 1).

The majority of the spectral lines studied were regis-

tered at the first and second order of diffraction of the monochromator 2. As we have already said, the measurements at the first order are necessary to obtain the relative intensity. The measurements at the second order give greater spectral resolution and, as such, are more useful in the determination of the Stark parameters. Besides the lines studied of Xe II, spectra of the 5016-Å line of He I in the high resolution monochromator were taken in order to contrast the density measurements obtained from the interferograms.

## III. NUMERICAL TREATMENT OF THE DATA

### A. Spectroscopic data processing

#### 1. *Adjustment of spectral profiles*

All the spectra have been fitted to a function of this type,

$$I(\lambda) = F_0 + F_1\lambda + \sum_\ell \frac{I_\ell + A_\ell(\lambda - \lambda_\ell)/a_\ell}{\left(\frac{\lambda - \lambda_\ell}{a_\ell}\right)^2 + 1}, \qquad (1)$$

with $F_0$, $F_1$, $I_\ell$, $A_\ell$, $\lambda_\ell$, and $a_\ell$ the adjustment parameters and where the sum is extended to all the lines that appear in the same spectrum. A fit of this kind permits an accurate determination of all the spectral line parameters: intensity, center, asymmetry, and width. In particular, the area under each line, obtained in this way, is not perturbed by neighboring lines. Each spectrum has been corrected for thermic and luminous background, which is not uniform throughout the detector. The fit was done in an interactive way with a very quick computer [14], which allows us to modify the parameters of the fit according to the operator instructions, showing on the screen the results of the fit as well as the quadratic dispersion between the experimental data and the calculated results. The area under each spectral line is obtained from the relation $\mathcal{A}_\ell = \pi I_\ell a_\ell / S(\lambda_\ell)$, where $S(\lambda_\ell)$ is the spectral response of the whole detecting system, which was obtained as mentioned above with the help of an incandescent calibrated lamp. The asymmetry parameter $A_\ell$, which does not appear in the area calculations, was never greater than 12 %. This algorithm, which we have used in the fit, allows us to resolve with accurary spectral lines which can be considerably overlapped (see Fig. 2). Each

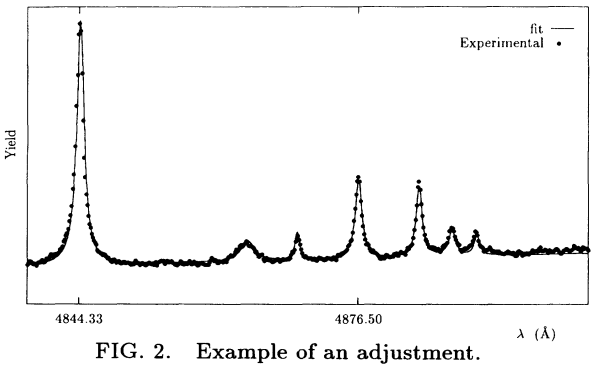


FIG. 2. Example of an adjustment.

record of the OMA2 is processed individually, which in this case means adjusting more than 1500 spectra interactively. The influence of the adjustment on the final results, both of the operator and the algorithm, has been contrasted and has been found to be less than the experimental error [15].

#### 2. *Instrumental function and Doppler broadening*

To ensure that only the Stark broadening of the investigated lines was taken into account, all the profiles have been corrected for instrumental and Doppler broadening, using the standard deconvolution procedure for Voigt profiles[16]. The instrumental profile was estimated by the maker to be about 2 or 3 channels; however, any misalignment can cause an increase of this. To achieve a realistic value, we have considered that the instrumental profile is essentially Gaussian and its width was determined by comparison between the results, obtained for the same spectral line, at the first and second diffraction order that must be the same. With this criterion, we have been able to establish an instrumental profile which has a Gaussian shape and a full width at half maximum (FWHM) of 3.5 channels.

#### 3. *Self-absorption*

In the data analysis, the spectra taken with and without the mirror M1 are compared to obtain the optical depth of the plasma for each spectral line. In none of the investigated lines have we found any evidence of self-absorption.

### B. Interferometric data processing

The computer analysis of the interferograms was done in different phases. First, each interferogram was corrected for electrical and luminous background (which was measured without the laser). The corrected inteferograms presented a drastic loss of contrast during the first instant of the plasma life; this loss of contrast is problably due to a slow response of the detector-amplifier system, because the amplitude of the interferometric fringes gets smaller as its frequency increases. To avoid this problem, we calculated the envelope of the interferogram so as to be able to normalize the maxima to $+1$ and the minima to $-1$, and in this way we avoid the contrast losses. We take the final part of each interferogram as the origin of phase because it is a stable interferencial state. In this way, we constructed a harmonic function of temporal variable frequency from which it was possible to get the phase difference between the two interference beams. The total refractivity of the plasma is related to the phase by the following relation [17]:

$$\Psi = \frac{2\pi}{\lambda} 2L(n-1)_e, \qquad (2)$$

where $L$ is the length of the plasma column, $\lambda$ is the He-Ne laser wavelength, and $n$ is the plasma refraction index.

Contrary to the adjustments of the spectra, all the interferograms contain the same information and, consequently, it is possible to control the repetitiveness of the system between discharges. Once the repetitiveness of the discharges has been verified, the phase is obtained by taking the average of the results from some 1500 interferograms.

## IV. DETERMINATION OF THE ELECTRON DENSITY

Interferometric methods give a very high accuracy; they are based on the measurement of the total refractivity of the plasma under study. The total refractivity of a low-density plasma can be obtained as the sum of the refractivities of each species in the plasma, in all their different ionization states. Among the different species, free electrons have the most important contribution to the plasma refractivity, this contribution is a function of the interferometer laser wavelength. The contribution of other species is not only very small, but it also depends very weakly on the wavelength. In our case, with helium plasma, it has been verified [12] that the refractivity due to neutral atoms is insignificant to all effects and, as a consequence, the refractivity obtained corresponds exclusively to the free electrons. Therefore, the electron density was obtained by[17]

$$(n-1)_e = -\frac{q_e^2 N_e \lambda^2}{8\pi^2 \epsilon_0 m_e c^2}, \tag{3}$$

where $q_e$ and $m_e$ are the charge and the electron mass in MKS units, respectively. The effective plasma length, one of the principal sources of error in the interferometric measurements, was taken as the distance between the lamp windows, i.e., 175 mm.

Also, we have checked the electron density by measuring the He I 5016-Å line calibrated in a previous work [10, 12]. This check has been carried out several times throughout the experiment.

Figure 3 shows the results for the electron densities obtained by both methods. From this plot it is clear that in the first moments of the plasma life, roughly until 70 $\mu$s, the electron density obtained interferometrically gives greater values than the density obtained spectroscopically. The agreement between the values provided by the two methods is very good the rest of the time. This agreement allows us to assure that, unless measured in these moments, we have taken the correct plasma length. In order to avoid this discrepancy, the results that we are going to discuss in the following sections are all results taken for $t > 70\,\mu s$ and from the interferometric measurements (because they have a greater precision). Precision was found to be better than 5% for the interferometric measurements and 15% for the electron density determined by spectroscopy [10].

For these differences in the electron densities in the first moments obtained by the two methods, we have proposed two hypotheses. The first one was a possible pinch effect produced in the first moments. However, after having taken radial measurements of the electron density, we

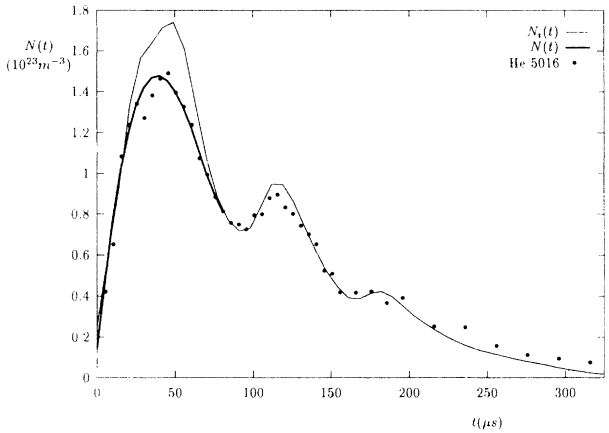


FIG. 3. Evolution of the electron density of the plasma. The fine outline indicates the density obtained from the interferograms. The dots correspond to the data calculated from the 5016-Å line of He I. The broad outline is a softened curve of these latter values.

can conclude that this effect does not appear in our plasmas during the investigated times nor in the area near the lamp axis. The second hypothesis is the possible variation of the effective plasma length during the experiment due to the existence of cold boundary layers. This second hypothesis has not been investigated yet.

The range of electron densities varies over (0.2–1.8) $\times 10^{23}$ m$^{-3}$.

## V. DETERMINATION OF ELECTRON TEMPERATURE AND CALCULATION OF TRANSITION PROBABILITIES

The light intensity emitted by the plasma corresponding to the transition between levels $i$ and $j$ of the emitting atom is given by the expression

$$I_{ij} = \frac{1}{4\pi} A_{ij} \hbar \omega_{ij} N_i = \frac{1}{2} A_{ij} \frac{\hbar c}{\lambda_{ij}} N_i\,, \tag{4}$$

where $A_{ij}$ is the transition probability between states $i$ and $j$, $\omega_{ij}$ the frequency emitted, and $N_i$ the population of highest level. This expression corresponds to the spontaneous emission. In our case the stimulated emission is of little importance as the typical radiation atom interaction is minimal. The population $N_i$ depends on the occupation temperature $T$ of the levels in this way,

$$N_i = N \frac{g_i \exp(-E_i/kT)}{Z(T)}\,, \tag{5}$$

$N$ being the total population of atoms in the emitting species, $g_i$ the degeneration of level $i$, $E_i$ the energy of said level, and $Z(T)$ the partition function of the emitting atom. Grouping these two expressions we get

$$I_{ij} = N\frac{g_i\hbar c}{2\lambda_{ij}}A_{ij}\frac{\exp(-E_i/kT)}{Z(T)}. \quad (6)$$

Calculating the temperature from expression (6) requires, among other things, the value of $I_{ij}$ in absolute units, which involves a costly process which is sometimes imprecise. With measurements of relative intensity, it is usual to establish relationships between different spectral lines in order to eliminate unknown common terms: the method known as the *Boltzmann plot*. In both methods it is absolutely necessary to know the transition probabilities of the lines under study and in our case, the data provided by the references cited herein are few and not very precise. As an alternative to these procedures we propose a method which allows us to obtain, under certain conditions, the plasma temperature and transition probabilities simultaneously. This method takes into account the experimental data corresponding to the spectral lines whose transition probability is unknown. We will find a curve pattern which accounts for the plasma temperature evolution against time from the intensity curves of the spectral lines. This curve and global evaluation of the transition probability data of some spectral lines allow us to fit the experimental data and to determine with this the plasma temperature in each temporal instant. In order that the proposed method is operational, it is necessary to have available measurements of different spectral lines measured under identical experimental conditions. It is also necessary to have these data under different experimental conditions. In our experiment, this is achieved by recording the spectra from different instants in the lifetime of the plasma.

### A. A curve pattern of the line intensity

By grouping constants in expression (6) we can write

$$I_{ij}(t) = C_{ij}\frac{N\exp[-\beta(t)E_i]}{Z(T)}, \quad (7)$$

where $\beta \equiv 1/kT$. We are going to consider, for now, that the dependence of the quotient $N/Z(T)$ on the temperature is much less abrupt than an exponential function, so that we can consider it as constant in time and, of course, independent of the spectral line. To simplify the formula a little we take the quotient $N/Z(T)$ as $C_{ij}$. Later on, in Sec. V B, we will analyze this simplification. With these hypotheses, the plasma temperature can be obtained from the relationship

$$\exp[-\beta(t)] = \left[\frac{I_{ij}(t)}{C_{ij}}\right]^{1/E_i}. \quad (8)$$

The first component of expression (8) is independent of the spectral line being studied and must be common to all the measured transitions. The constant $C_{ij}$ which appears in the second component depends on the transition probability, which, in principle, is unknown to us. We separate the second component of (8) into two factors, one of them independent of time, fixed for each spectral line:

$$\exp[-\beta(t)] = K_{ij}\,[I_{ij}(t)]^{1/E_i},$$
$$K_{ij} \equiv \left[\frac{N}{Z(T)}\frac{g_i\hbar cA_{ij}}{2\lambda_{ij}}\right]^{-1/E_i}. \quad (9)$$

Our unknown factors are then the value of $\exp[-\beta(t)]$ in each instant $t$ and the value $K_{ij}$ for each spectral line. The data we have available allow us to calculate $[I_{ij}(t)]^{1/E_i}$ for each spectral line and in each instant $t$. To simplify we will indicate the subindices $_{ij}$ with $_\ell$, which covers all the spectral lines measured. Given that the relationship (8) has to be fulfilled indendepent of the line being considered, we will ensure that the quadratic dispersion is minimal:

$$H = \sum_\ell \sum_t \sum_r \left\{K_\ell\,[I_{\ell r}(t)]^{1/E_\ell} - \exp[-\beta(t)]\right\}^2, \quad (10)$$

where the sum of $\ell$ is extended to all the spectral lines considered, $\sum_t$ covers all the temporal instants in which there is spectral measurement, and $\sum_r$ covers all the records obtained for a given line in a given temporal instant. In our case 21 different spectral lines were studied in 55 different temporal instants. For each spectral line and temporal instant there is varying number of measurements. The total number of records used were 1312.

For means of simplification, we take

$$\mathcal{E}(t) \equiv \exp[-\beta(t)],$$
$$\mathcal{I}_{\ell r}(t) \equiv [I_{\ell r}(t)]^{1/E_\ell}, \quad (11)$$

and we find the minimum of $H$ selecting the values of $K_\ell$ and $\mathcal{E}(t)$ for each value of $(t)$ in such a way that

$$\frac{\partial H}{\partial K_\ell} = 0 \implies K_\ell = \frac{\sum_t \sum_r \mathcal{I}_{\ell r}(t)\mathcal{E}(t)}{\sum_t \sum_r \mathcal{I}_{\ell r}(t)^2}, \quad (12)$$

$$\frac{\partial H}{\partial \mathcal{E}(t)} = 0 \implies \mathcal{E}(t) = \frac{\sum_\ell K_\ell \sum_r \mathcal{I}_{\ell r}(t)}{n(t)}, \quad (13)$$

where $n(t)$ is the total number of records in the instant $t$. Incorporating (12) and (13) we have

$$\mathcal{E}(t) = \sum_\ell \frac{\sum_r \mathcal{I}_{\ell r}(t)}{n(t)}\left[\frac{\sum_{t'}\sum_{r'}\mathcal{E}(t')\mathcal{I}_{\ell r'}(t')}{\sum_{t''}\sum_{r''}\mathcal{I}_{\ell r''}(t'')^2}\right]$$

$$= \frac{1}{n(t)}\sum_{t'}\mathcal{E}(t')\sum_\ell \frac{\sum_r \mathcal{I}_{\ell r}(t)\sum_{r'}\mathcal{I}_{\ell r'}(t')}{\sum_{t''}\sum_{r''}\mathcal{I}_{\ell r''}(t'')^2}. \quad (14)$$

We define the quantities

$$b_{tt'} = \sum_{\ell} \frac{\sum_{r} \mathcal{I}_{\ell r}(t) \sum_{r'} \mathcal{I}_{\ell r'}(t')}{\sum_{t''} \sum_{r''} \mathcal{I}_{\ell r''}(t'')^2},$$

$$a_{tt'} = \begin{cases} b_{tt'} - n(t) & \text{if } t = t' \\ b_{tt'} & \text{if } t \neq t', \end{cases} \tag{15}$$

which are calculated directly from the experimental data $\mathcal{I}_{\ell r}(t)$. With this notation Eq. (14) is reduced to

$$\sum_{t'} a_{tt'} \mathcal{E}(t') = 0. \tag{16}$$

We find ourselves with a homogenous system as a consequence of which the values of $K_\ell$ and $\mathcal{E}(t)$ can both be multiplied by an arbitrary factor, without the minimun calculation we are making being modified; see (9). This indetermination, as is logical, only results in a scale factor of function $\mathcal{E}(t)$, which we are trying to determine. In order to continue with the calculation we must fix a scale, which we can do arbitrarly, taking $\mathcal{E}(t_m) = 1$ for a certain value of $t_m$, for example, that which corresponds to the instant of maximum intensity of the most intense line. With this, the system (16) is written

$$\sum_{t' \neq t_m} a_{tt'} \mathcal{E}(t') = -a_{tt_m}, \qquad t \neq t_m. \tag{17}$$

The equation system (17)—in our case of (54) equations with (54) unknown factors—provides a normalized temporal evolution curve $\mathcal{E}(t)$ which only depends on the temperature and not on the characteristics of each spectral line. Once the system is resolved and a curve pattern of $\mathcal{E}(t)$ is obtained, we can verify the curve $\beta(t)$ taking logarithms, which gives us the inverse of the temperature; the additive indeterminate constant is unknown. To determine this constant we need to relate the values of $K_\ell$ to some known quantities. The method we propose is based on the consideration that the available data of transition probabilities, although not very precise, are globally valid. Taking into account that

$$K_{\ell:i\to j} = \chi \left[ \frac{2\lambda_{ij} Z(T)}{N g_i \hbar c A_{ij}} \right]^{1/E_i}, \tag{18}$$

where $\chi$ is the unknown scale factor, we can define the quantities

$$B_{\ell:i\to j} \equiv \left[ \frac{2\lambda_{ij}}{g_i \hbar c A_{ij}} \right]^{1/E_i},$$

$$Y_\ell \equiv \frac{K_\ell}{B_\ell} = \chi \left[ \frac{Z(T)}{N} \right]^{1/E_\ell}. \tag{19}$$

Taking logarithms in this last expression

$$y_\ell = \ln(Y_\ell) = \ln(\chi) + \frac{1}{E_\ell} \ln\left( \frac{Z(T)}{N} \right) \tag{20}$$

gives us a linear relationship between the known quantities $y_\ell$ and $1/E_\ell$, which we can fit for minimun squares. The values of the fitting give us the constant $\chi$ and the relationship $Z(T)/N$; the constant factor is unknown, which accounts for the density of emitters in the plasma.

### B. Behavior of quotient $N/Z(T)$

Expression (20) allows us to establish, except for an unknown multiple constant, an average value of the relationship $N/Z(T)$. In our case, the quantity $N$, which accounts for the global population of the emitting species, refers to the xenon once ionized. It is a magnitude, therefore, which strongly depends on the temperature. But this strong dependency is included also in $Z(T)$, in the form of a factor $\exp(-E_{\text{ion}}/k)$, where $E_{\text{ion}}$ is the ionization potential of the xenon. Therefore, in a wide range of temperatures, the quotient $N/Z(T)$ is practically a constant. Bear in mind that our plasma is dominated by helium, which supplies the free electrons and acts as a buffer gas in such a way that the population of the ionized xenon remains stable.

Nevertheless, this hypothesis can be proved at a later stage once the relative value of $N/Z(T)$ is obtained from expression (20). To do this, different fitting procedures have been carried out as described in Sec. V A, taking only a reduced temporal interval, so that it covers a narrow range of temperatures. This range should be narrow enough to be able to consider that the temperature does not change significantly, but wide enough to cover different experimental conditions, given that this is necessary for the fitting method to work. Specifically, if the total duration of the plasma lifetime is divided into five equal parts —see Fig. 4— values of $N/Z(T)$ are obtained which in the last four intervals —between 60 and 300 $\mu$s— fluctuate below 4%. In the interval from 0 to 60 $\mu$s, the value of $N/Z(T)$ proves to be 80% of the average total value and between 60 and 300 $\mu$s it varies between 145% and 151%. Such an apparently great difference does not result in an important modification of the results. In this same procedure, the transition probabilities obtained for the 21 spectral lines dealt with in the five calculations carried out differ among themselves in values of around 4%; in 10 of the spectral lines it did not reach 4%. The greatest dispersion is found in the 4890-Å line and is 11%. This is

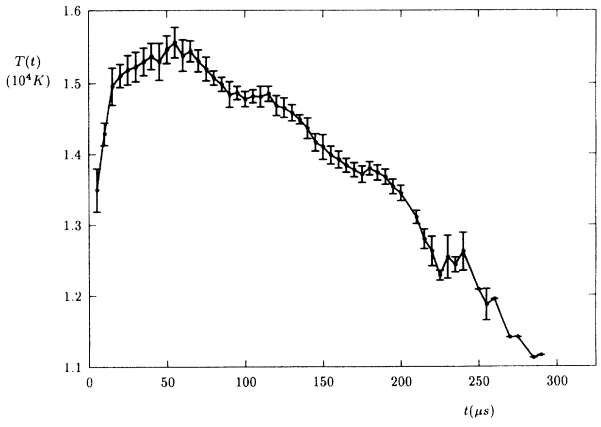


FIG. 4. Evolution of the plasma temperature.

an expected consequence of the method used. The value $N/Z(T)$ obtained from expression (20) is an average of this quantity in the whole temporal interval fitted.

## VI. RESULTS

### A. Temperature and transition probabilities

Figure 4 shows the results obtained in determining the curve pattern of the normalized line intensities by the energy of the upper level. To obtain this curve the data from 33 temporal sequences corresponding to 21 different transitions were used. Each temporal sequence has between 30 and 80 items of data, according to the spectral line. In the fitting of expression (20) the transition probabilities of nine spectral lines tabulated in Ref. [18] were used, their being a group data selected by the compilation authors. The final calculation is shown in the figure, that is to say, this curve pattern is expressed in terms of the temperature values. The figure also shows the average dispersion between the individual values and the average curve. The small amount that the data of each line deviates from the average results is in itself good news, given that it reflects the fact that all of the evolution curves of line intensity correctly reproduce the type of function that can theoretically be expected, that is to say, in the form $I^{1/E}$.

Figure 5 shows the values of $y_\ell$ versus $1/E_\ell$ and the linear fitting of expression (20). With this fitting we fix the value of $\chi$, with which we obtain the temperature from the curve pattern

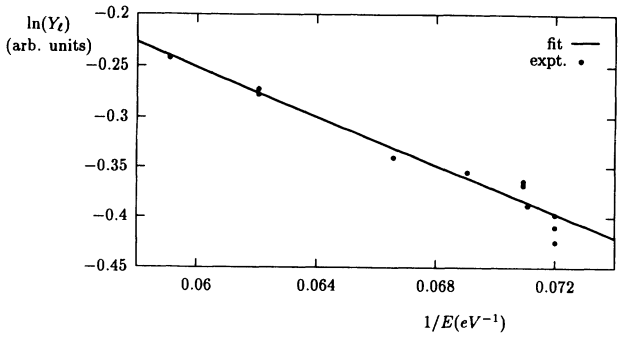


FIG. 5. Fitting to determine $\chi$.

$$T(t) = \frac{-1}{k \ln[\chi \mathcal{E}(t)]} . \tag{21}$$

The calculation carried out allows us to find the transition probabilities of all of the lines that have been used in the determination of the intensity curve pattern. The results are shown in Table I. As is obvious, our results basically agree with those in Ref. [18] given that these are those used in order to scale the values of $A_{ij}$ in the fitting of expression (20). Good agreement is observed with the data in Ref. [19] and for wavelengths less than 5000 Å, and also with the data in Ref. [20]. At greater wavelengths the data of Ref. [20] are notably greater without there being a reason for this discrepancy. We have carried out a fitting equivalent to that shown in

TABLE I. Transition probabilities in units of $10^8\ s^{-1}$ corresponding to the spectral lines indicated. The values of Ref. [18] are those which have been used in the fitting.

| Spectral line (Å) | | $A_{ij}$ ($10^8\ s^{-1}$) | | | | | | |
|---|---|---|---|---|---|---|---|---|
| | | Ref. [18] | This work | Ref. [19] | Ref. [20] | Ref. [22] | Ref. [23] | Ref. [24] |
| 4330.52 | $6p\,^4D^0_{5/2}$–$6d\,^4F_{7/2}$ | 1.4 | 1.46 | | 1.29 | | 0.337 | |
| 4585.48 | $6s\,^4D^0_{7/2}$–$6d\,^4D_{7/2}$ | | 0.620 | | 1.01 | | 0.0424 | |
| 4592.05 | $6p\,^4S^0_{3/2}$–$6d\,^4P_{5/2}$ | | 0.883 | | 0.89 | | | |
| 4603.03 | $6s\,^4P_{3/2}$–$6p\,^4D^0_{3/2}$ | 0.82 | 0.753 | 1.356 | 0.69 | 1.28 | 1.22 | 0.49 |
| 4615.50 | $6s'\,^2D_{5/2}$–$6p'\,^2P^0_{3/2}$ | | 0.386 | | 0.30 | | 0.0264 | |
| 4844.33 | $6s\,^4P_{5/2}$–$6p\,^4D^0_{7/2}$ | 1.1 | 0.868 | 1.475 | 0.77 | 4.3 | 0.127 | 1.66 |
| 4862.54 | $6p\,^4P^0_{5/2}$–$7s\,^4P_{5/2}$ | | 0.670 | | 0.72 | | | |
| 4876.50 | $5d\,^2D_{5/2}$–$6p'\,^2F^0_{7/2}$ | 0.63 | 0.622 | | 0.94 | | | |
| 4883.53 | $6s\,^4P_{1/2}$–$6p\,^4S^0_{3/2}$ | | 0.670 | 1.101 | 0.77 | | 0.172 | |
| 4887.30 | $6s\,^2P_{3/2}$–$6p\,^2P^0_{3/2}$ | | 0.267 | 0.557 | 0.42 | | | |
| 4890.09 | $6s\,^4P_{5/2}$–$6p\,^4D^0_{5/2}$ | | 0.087 | 0.055 | 0.10 | | | |
| 4988.77 | $6s\,^2P_{1/2}$–$6p\,^2D^0_{3/2}$ | | 0.209 | 0.792 | 0.35 | | | |
| 5292.22 | $6s\,^4P_{5/2}$–$6p\,^4P^0_{5/2}$ | 0.89 | 0.904 | 1.095 | 2.32 | 4.6 | 0.082 | 1.77 |
| 5309.27 | $6s\,^2P_{3/2}$–$6p\,^4S^0_{3/2}$ | | 0.223 | 0.226 | 0.94 | | | |
| 5313.87 | $6p\,^4D^2_{7/2}$–$7s\,^4P_{5/2}$ | | 0.889 | | 3.46 | | | |
| 5339.38[a] | $6s\,^4P_{5/2}$–$6p\,^4P^0_{3/2}$ | | 0.669 | 0.868 | 1.88 | | 0.238 | |
| 5419.15 | $6s\,^4P_{3/2}$–$6p\,^4D^0_{5/2}$ | 0.62 | 0.649 | 1.018 | 2.13 | 3.26 | | |
| 5438.96 | $6s\,^2P_{3/2}$–$6p\,^2S^0_{1/2}$ | 0.74 | 0.855 | 1.016 | 3.76 | | | |
| 5460.39 | $5d\,^4D_{5/2}$–$6p\,^4D^0_{7/2}$ | | 0.064 | | 0.27 | | | |
| 6036.20 | $5d\,^4D_{5/2}$–$6p\,^4P^0_{5/2}$ | 0.075 | 0.111 | | 0.15 | | | |
| 6051.15 | $5d\,^4D_{7/2}$–$6p\,^4P^0_{5/2}$ | 0.17 | 0.205 | | 0.52 | | 0.80 | 1.93 |

[a]Doubly classified line.

Fig. 5, taking the data from Ref. [20]. The result shows a correlation of a quality notably inferior to that observed in Fig. 5. This once again justifies the selection of the group of data taken to scale the transition probabilities and, in general, the validity of the proposed method to simultaneously determine the transition probabilities and the plasma temperature.

### B. Stark width

Figure 6 shows the values obtained of the full width at half maximum in a typical case. The behavior of all the lines is anologous and we have never observed dependences that are not lineal between the width and the quotient $N_e/\sqrt{T}$ [21]. A tendency of the linewidth to decrease proportionately as the temperature increases is systematically observed. Nevertheless, the reduced range of temperatures prevents us from fixing experimentally the functional dependence of the width on the temperature. When the width divided by $N_e/\sqrt{T}$ is analyzed, the experimental data do not present any detectable systematic tendency with the density or the temperature.

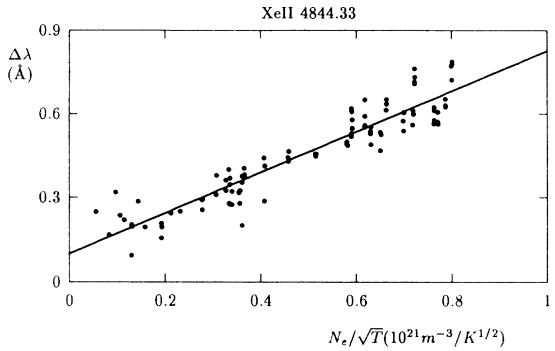


FIG. 6. Full width at half maximum of the line Xe II 4844.33-Å line vs $N_eT^{-1/2}$. The straight line is the fitting for minimum squares.

In Table II the results of the full width at half maximum of all the spectral lines under study are summarized. A variable number of measurements for each spectral line were taken at the intervals of density and temperature specified in the table. With the width data obtained a lineal fitting was made against $N_e/\sqrt{T}$. The expected

TABLE II. Experimental Stark widths (FWHM) of xenon II lines in Å. $n$: number of spectra used; $N_{\max}$ ,$N_{\min}$, $T_{\max}$, $T_{\min}$: intervals of density and temperature; $\langle N_e\rangle$, $\langle T\rangle$, $\langle\Delta\lambda_{1/2}\rangle$: average values of the density, temperature, and total width; $\sigma_{\Delta\lambda}$: estimated error of measurement. The asterisk denotes an ordinate observed at the origin between 15% and 30%.

| Spectral line (Å) | | n | $N_{\min}$–$N_{\max}$ | $T_{\min}$–$T_{\max}$ | $\langle N_e\rangle$ | $\langle T\rangle$ | $\Delta\lambda_{1/2}\pm\sigma_{\Delta\lambda}$ |
|---|---|---|---|---|---|---|---|
| 4330.52 | $6p\,^4D^0_{5/2}$–$6d\,^4F_{7/2}$ | 22 | 0.38–0.99 | 13.7–15.3 | 0.77 | 14.7 | 1.282 ±0.08 |
| 4585.48 * | $6s\,^4D^0_{7/2}$–$6d\,^4D_{7/2}$ | 8 | 0.71–0.99 | 14.7–15.3 | 0.81 | 14.9 | 1.266 ±0.14 |
| 4592.05 * | $6p\,^4S^0_{3/2}$–$6d\,^4P_{5/2}$ | 24 | 0.35–0.99 | 13.5–15.3 | 0.75 | 14.7 | 1.895 ±0.07 |
| 4603.03 | $6s\,^4P_{3/2}$–$6p\,^4D^0_{3/2}$ | 25 | 0.23–0.99 | 12.7–15.3 | 0.73 | 14.6 | 0.420 ±0.03 |
| 4615.50 | $6s'\,^2D_{5/2}$–$6p'\,^2P^0_{3/2}$ | 8 | 0.71–0.99 | 14.7–15.3 | 0.81 | 14.9 | 0.775 ±0.17 |
| 4844.33 | $6s\,^4P_{5/2}$–$6p\,^4D^0_{7/2}$ | 98 | 0.11–0.99 | 11.1–15.3 | 0.60 | 14.1 | 0.466 ±0.05 |
| 4862.54 | $6p\,^4P^0_{5/2}$–$7s\,^4P_{5/2}$ | 73 | 0.14–0.99 | 12.5–15.3 | 0.63 | 14.3 | 1.030 ±0.14 |
| 4876.50 | $5d\,^2D_{5/2}$–$6p'\,^2F^0_{7/2}$ | 73 | 0.14–0.99 | 12.5–15.3 | 0.63 | 14.3 | 0.301 ±0.01 |
| 4883.53 | $6s\,^4P_{1/2}$–$6p\,^4S^0_{3/2}$ | 73 | 0.14–0.99 | 12.5–15.3 | 0.63 | 14.3 | 0.325 ±0.02 |
| 4887.30 | $6s\,^2P_{3/2}$–$6p\,^2P^0_{3/2}$ | 72 | 0.14–0.99 | 12.5–15.3 | 0.64 | 14.3 | 0.353 ±0.03 |
| 4890.09 * | $6s\,^4P_{5/2}$–$6p\,^4D^0_{5/2}$ | 72 | 0.14–0.99 | 12.5–15.3 | 0.64 | 14.3 | 0.337 ±0.07 |
| 4919.66 | $6s\,^2P_{1/2}$–$6p\,^2P^0_{1/2}$ | 16 | 0.38–0.99 | 13.6–15.3 | 0.74 | 14.6 | 0.472 ±0.12 |
| 4921.48 | $6s\,^2P_{3/2}$–$6p\,^2D^0_{5/2}$ | 18 | 0.26–0.99 | 13.0–15.3 | 0.70 | 14.5 | 0.372 ±0.03 |
| 4988.77 | $6s\,^2P_{1/2}$–$6p\,^2D^0_{3/2}$ | 40 | 0.23–0.99 | 12.7–15.3 | 0.70 | 14.5 | 0.778 ±0.10 |
| 4991.17 | $6p'\,^2P^0_{3/2}$–$6d'\,^2D_{5/2}$ | 14 | 0.61–0.99 | 14.3–15.3 | 0.88 | 14.8 | 2.881 ± 0.8 |
| 5260.44 | $6s\,^2P_{1/2}$–$6p\,^2P^0_{3/2}$ | 14 | 0.39–0.99 | 13.7–15.3 | 0.75 | 14.7 | 0.525 ±0.04 |
| 5261.95 | $6s'\,^2D_{3/2}$–$6p'\,^2D^0_{3/2}$ | 14 | 0.39–0.99 | 13.7–15.3 | 0.75 | 14.7 | 0.367 ±0.03 |
| 5292.22 * | $6s\,^4P_{5/2}$–$6p\,^4P^0_{5/2}$ | 37 | 0.06–0.98 | 11.1–15.3 | 0.66 | 14.3 | 0.501 ±0.02 |
| 5309.27 * | $6s\,^2P_{3/2}$–$6p\,^4S^0_{3/2}$ | 25 | 0.19–0.98 | 12.3–15.3 | 0.67 | 14.4 | 0.394 ±0.06 |
| 5313.87 | $6p\,^4D^2_{7/2}$–$7s\,^4P_{5/2}$ | 25 | 0.19–0.98 | 12.3–15.3 | 0.67 | 14.4 | 1.288 ±0.09 |
| 5339.38[a] | $6s\,^4P_{5/2}$–$6p\,^4P^0_{3/2}$ | 45 | 0.19–0.98 | 12.3–15.3 | 0.69 | 14.4 | 0.427 ±0.02 |
| 5368.07 * | $5d\,^2P_{1/2}$–$6p\,^2P^0_{1/2}$ | 7 | 0.71–0.95 | 14.5–14.9 | 0.79 | 14.8 | 0.473 ±0.13 |
| 5372.39 | $6s\,^4P_{3/2}$–$6p\,^4P^0_{1/2}$ | 18 | 0.26–0.99 | 13.0–15.3 | 0.70 | 14.5 | 0.408 ±0.03 |
| 5419.15 | $6s\,^4P_{3/2}$–$6p\,^4D^0_{5/2}$ | 42 | 0.07–0.98 | 11.3–15.3 | 0.65 | 14.3 | 0.545 ±0.03 |
| 5438.96 * | $6s\,^2P_{3/2}$–$6p\,^2S^0_{1/2}$ | 65 | 0.11–0.98 | 11.8–15.3 | 0.66 | 14.3 | 0.404 ±0.02 |
| 5460.39 | $5d\,^4D_{5/2}$–$6p\,^4D^0_{7/2}$ | 39 | 0.11–0.98 | 11.8–15.3 | 0.67 | 14.4 | 0.437 ±0.02 |
| 5472.61 | $5d\,^4D_{7/2}$–$6p\,^4D^0_{7/2}$ | 15 | 0.38–0.98 | 13.6–15.3 | 0.73 | 14.6 | 0.430 ±0.02 |
| 5976.46 | $6s\,^4P_{3/2}$–$6p\,^4P^0_{3/2}$ | 16 | 0.26–0.98 | 13.0–15.3 | 0.70 | 14.5 | 0.450 ±0.03 |
| 6036.20 * | $5d\,^4D_{5/2}$–$6p\,^4P^0_{5/2}$ | 33 | 0.21–0.99 | 12.5–15.3 | 0.73 | 14.6 | 0.536 ±0.04 |
| 6051.15 | $5d\,^4D_{7/2}$–$6p\,^4P^0_{5/2}$ | 33 | 0.21–0.99 | 12.5–15.3 | 0.73 | 14.6 | 0.554 ±0.02 |

[a]Doubly classified line.

value of this fitting for the average conditions in density and temperature in each spectral line is presented in the table. The error assigned to our measurements fundamentally come from the dispersion of the data obtained in the lineal fitting. On average, it proves to be in the region of 7%, although with a strong dependence on the spectral line. The errors of a systematic nature, such as those produced by the spectrometer resolution, data processing, etc., are estimated to be less than 1% and have been considered in calculating the tabulated error.

In order to be able to compare our results with those of the bibliography, all the data have been normalized to $N_e = 10^{23}$ m$^{-3}$, $T = 10^4$ K (see Table III). Our values are the result of an extrapolation applied to these conditions by means of the lineal fitting of the width against $N_e/\sqrt{T}$. The data of the other authors [1–4, 7–9], given that we do not have sufficient data available in order to carry out this fit, have been normalized by simply dividing their values by $N_e/\sqrt{T}$. In the majority of the cases, this normalization did not substantially modify the values as the chosen conditions are close to those typical of the data of the bibliography. Both methods would lead to practically the same results if the ordinate at the origin of regression were insignificant. This behavior was not observed in all the cases [5]. In our case, this said ordinate takes values in the region of the experimental error. For the lines marked by an asterisk in Table II, an ordinate at the origin between 15% and 30% has been observed.

Vitel and Skowronek [5], working with a flash tube, measured the widths and shifts for four Xe II lines (all of them have been measured in the present work). They give, for each line, numerical results at five different electron densities and temperatures, in ranges of $(4.5 - 13.4) \times 10^{23}$ m$^{-3}$ and 12 600–15 800 K, respectively. A high ordinate at the origin is interpreted by the authors as an effect of the lack of linearity of the Stark width in proportion to the increase of electron density. Given that the authors provide a sufficient quantity of data, we have carried out a lineal fitting like the one indicated

TABLE III. Comparison between different authors of the "normalized" broadening (in Å) at $N_e = 10^{23}$ m$^{-3}$, $T = 10\,000$ K, of the Xe II lines. The lines indicated by $N$ and $T$ account for the range of electron densities (in $10^{23}$ m$^{-3}$) and the temperatures (in $10^3$ K), respectively of the cited author.

| | Ref | This work | [1] | [2] | [3] | [4] | [5] | [6] | [7] | [8] | [9] |
|---|---|---|---|---|---|---|---|---|---|---|---|
| | $N_{min}$ | 0.1 | 1.0 | 0.6 | 0.1 | 0.64 | 4.7 | 0.28 | 0.5 | 9 | 0.27 |
| | $N_{max}$ | 1.0 | 1.0 | 1.8 | 1.5 | 1.5 | 13.4 | 2.2 | 2.0 | 11 | 0.27 |
| Spectral | $T_{min}$ | 11 | 11 | 10.2 | 7.8 | 9.4 | 12.6 | 9.0 | 10 | 12.5 | 14.5 |
| line (Å) | $T_{max}$ | 16 | 11 | 12.4 | 8.4 | 10.7 | 15.8 | 16 | 12 | 13 | 14.5 |
| 4330.52 | | 1.916 | | | | | | | 1.38 | | |
| 4585.48 | | 1.455 | | | | | | | 1.38 | | |
| 4592.05 | | 2.703 | | | | | | | | | |
| 4603.03 | | 0.683 | 0.85 | 0.89 | | 0.436 | | | 0.68 | | 0.70 |
| 4615.50 | | 1.095 | | | | | | | | | |
| 4844.33 | | 0.826 | 0.85 | 0.91 | | 0.367 | 0.72 | | 0.75 | 0.62 | |
| 4862.54 | | 1.787 | | | | | | | | | |
| 4876.50 | | 0.550 | | | | 0.380 | | | | | |
| 4883.53 | | 0.542 | | | | 0.348 | | | | | 0.60 |
| 4887.30 | | 0.623 | | | | | | | | | 0.55 |
| 4890.09 | | 0.465 | | | | | | | | | 0.57 |
| 4919.66 | | 0.790 | | | | | | | | | 0.51 |
| 4921.48 | | 0.656 | | | | | | | 0.59 | | 0.68 |
| 4988.77 | | 1.314 | | | | 0.581 | | | | | 0.60 |
| 4991.17 | | 2.56 | | | | | | | | | |
| 5260.44 | | 0.866 | | | | 0.709 | | | | | 0.64 |
| 5261.95 | | 0.583 | | | | 0.615 | | | | | 0.66 |
| 5292.22 | | 0.805 | 0.92 | 0.98 | | 0.427 | 0.85 | | 0.83 | 0.67 | |
| 5309.27 | | 0.570 | | | | | | | | | |
| 5313.87 | | 2.183 | | | | | | | | | |
| 5339.38[a] | | 0.679 | | | 0.54 | | 0.914 | | 0.67 | 0.67 | |
| 5368.07 | | 1.027 | | | | | | | | | 0.58 |
| 5372.39 | | 0.690 | 0.88 | 0.95 | 0.60 | 0.480 | | | 0.68 | | 0.72 |
| 5419.15 | | 0.897 | 0.93 | 1.00 | 0.81 | 0.556 | 1.38 | 0.74 | | 0.76 | |
| 5438.96 | | 0.608 | | | 0.60 | 0.456 | | | 0.57 | | 0.71 |
| 5460.39 | | 0.749 | | | | | | | | | 0.66 |
| 5472.61 | | 0.682 | 0.94 | 1.02 | | 0.579 | | | 0.86 | | |
| 5976.46 | | 0.791 | | | | 0.575 | | | | | 0.86 |
| 6036.20 | | 0.769 | | | | 0.641 | | | 0.79 | | 0.69 |
| 6051.15 | | 0.855 | 0.95 | 1.02 | | 0.668 | | | 0.79 | | |

[a]Doubly classified line.

previously. With this method the values which appear in the table are obtained. If we take the quotient of the width between $N_e/\sqrt{T}$ values much lower values than those tabulated here are obtained.

The work by Manola *et al.* [6] is devoted to the study of the 5419-Å line. This work, which has been carried out in a shock tube, with a temperature range of 9025–16 200 K, and an electron density $(0.497 - 2.6) \times 10^{23}$ m$^{-3}$, shows the variation of the Stark broadening with the temperature. In this work, the authors establish a comparison with previous measurements [3] taken at lower temperatures. The discrepancy between both works is interpreted by the authors as a great decrease in the width with the increase in temperature. Nonetheless, the tabulated value has been obtained following the same criterion as in our work using their results from Table III in Ref. [6]. In both of the cases mentioned, the coefficient of lineal regression is excellent.

From the analysis of Table III it is deduced that the majority of the data are consistent, within experimental error, except for Nick and Helbig's results, which in certain cases result in an increase by a factor of 2. From an experimental point of view, the only relevant differences between this last work and the rest is the use of a continuous plasma with pure xenon, while the other authors, in general, use pulsed plasmas with mixtures of gases. This difference does not appear to justify such significant discrepancies.

### C. Stark shifts

In Table IV the results of Stark shifts obtained in the present work are compared with those from Ref. [5]. The data of Ref. [5] are obtained by taking the average of the quotients between the shifts and the density. Due to the fact that, in general, the shift of the lines under study is very little, the relative precision of our results is less than that obtained in the width. Nevertheless, a clear lineal dependency of the shifts on the density is systematically observed. It is not possible to appreciate any dependency on the temperature, so the results must be considered to have been taken at 15 000 K, which corresponds to the prevailing temperature in the experiment. The values which are tabulated are the results of the expected value for $N_e = 10^{23}$ m$^{-3}$ in a lineal fitting of the shifts against the density. The principal source of error is found in the precise determination of the center of the experimental profiles, due as much to its width as to the numerical algorithm uses to characterize it. Taking these considerations into account, 0.01 Å can be fixed as the absolute error in the measurements.

TABLE IV. Stark shift (in Å) of the line indicated for $N_e = 10^{23}$ m$^{-3}$, $T = 15\,000$ K.

| Spectral line (Å) | | Shift This work | Shift Ref. [5] |
|---|---|---|---|
| 4330.52 | $6p\,^4D^0_{5/2}$–$6d\,^4F_{7/2}$ | +0.68 | |
| 4585.48 | $6s\,^4D^0_{7/2}$–$6d\,^4D_{7/2}$ | +0.82 | |
| 4592.05 | $6p\,^4S^0_{3/2}$–$6d\,^4P_{5/2}$ | +0.85 | |
| 4603.03 | $6s\,^4P_{3/2}$–$6p\,^4D^0_{3/2}$ | $\lvert d\rvert < 0.01$ | |
| 4615.50 | $6s'\,^2D_{5/2}$–$6p'\,^2P^0_{3/2}$ | $\lvert d\rvert < 0.01$ | |
| 4844.33 | $6s\,^4P_{5/2}$–$6p\,^4D^0_{7/2}$ | −0.03 | −0.01 |
| 4862.54 | $6p\,^4P^0_{5/2}$–$7s\,^4P_{5/2}$ | +0.57 | |
| 4876.50 | $5d\,^2D_{5/2}$–$6p'\,^2F^0_{7/2}$ | −0.09 | |
| 4883.53 | $6s\,^4P_{1/2}$–$6p\,^4S^0_{3/2}$ | −0.14 | |
| 4887.30 | $6s\,^2P_{3/2}$–$6p\,^2P^0_{3/2}$ | $\lvert d\rvert < 0.01$ | |
| 4890.09 | $6s\,^4P_{5/2}$–$6p\,^4D^0_{5/2}$ | $\approx -0.06$ | |
| 4919.66 | $6s\,^2P_{1/2}$–$6p\,^2P^0_{1/2}$ | $\lvert d\rvert < 0.01$ | |
| 4921.48 | $6s\,^2P_{3/2}$–$6p\,^2D^0_{5/2}$ | −0.04 | |
| 4988.77 | $6s\,^2P_{1/2}$–$6p\,^2D^0_{3/2}$ | +0.29 | |
| 4991.17 | $6p'\,^2P^0_{3/2}$–$6d'\,^2D_{5/2}$ | +2.03 | |
| 5260.44 | $6s\,^2P_{1/2}$–$6p\,^2P^0_{3/2}$ | +0.02 | |
| 5261.95 | $6s'\,^2D_{3/2}$–$6p'\,^2D^0_{3/2}$ | $\lvert d\rvert < 0.01$ | |
| 5292.22 | $6s\,^4P_{5/2}$–$6p\,^4P^0_{5/2}$ | −0.07 | −0.05 |
| 5309.27 | $6s\,^2P_{3/2}$–$6p\,^4S^0_{3/2}$ | $\approx$ -0.06 | |
| 5313.87 | $6p\,^4D^2_{7/2}$–$7s\,^4P_{5/2}$ | +1.08 | |
| 5339.38[a] | $6s\,^4P_{5/2}$–$6p\,^4P^0_{3/2}$ | −0.08 | −0.07 |
| 5368.07 | $5d\,^2P_{1/2}$–$6p\,^2P^0_{1/2}$ | | |
| 5372.39 | $6s\,^4P_{3/2}$–$6p\,^4P^0_{1/2}$ | $\lvert d\rvert < 0.01$ | |
| 5419.15 | $6s\,^4P_{3/2}$–$6p\,^4D^0_{5/2}$ | −0.06 | −0.02 |
| 5438.96 | $6s\,^2P_{3/2}$–$6p\,^2S^0_{1/2}$ | −0.07 | |
| 5460.39 | $5d\,^4D_{5/2}$–$6p\,^4D^0_{7/2}$ | +0.11 | |
| 5472.61 | $5d\,^4D_{7/2}$–$6p\,^4D^0_{7/2}$ | +0.09 | |
| 5976.46 | $6s\,^4P_{3/2}$–$6p\,^4P^0_{3/2}$ | −0.09 | |
| 6036.20 | $5d\,^4D_{5/2}$–$6p\,^4P^0_{5/2}$ | +0.12 | |
| 6051.15 | $5d\,^4D_{7/2}$–$6p\,^4P^0_{5/2}$ | +0.08 | |

[a]Doubly classified line.

## ACKNOWLEDGMENTS

The authors thank Valentín Cardeñoso for his valuable collaboration in the software development, the Departamento de Ingeniería de Sistemas y Automática of Valladolid University for the use of their computers, Santiago González for his work in the experimental device assembly, and the Dirección General de Investigación Científica y Técnica (Ministerio de Educación y Ciencia) of Spain for its financial support under Contract No. PB-90-0353.

[1] A. Lesage, M. H. Miller, J. Richou, and Truong-Bach, *Spectral Line Shapes,* edited by B. Wende (de Gruyter, Berlin, 1981).
[2] M. H. Miller, A. Lesage, and D. Abadie, Phys. Rev A **25**, 2064 (1982).
[3] J. Richou, S. Manola, J. L. Lebrun, and A. Lesage, Phys. Rev. A **29**, 3181 (1984).
[4] K. P. Nick and V. Helbig, Phys. Scr. **33**, 55 (1986).
[5] Y. Vitel and M. Skowronek, J. Phys. B **20**, 6493 (1987).
[6] S. Manola, N. Konjevic, J. Richou, J. L. Lebrun, and A. Lesage, Phys. Rev. A **38**, 5742 (1988).
[7] A. Lesage, D. Abadie, and M. H. Miller, Phys. Rev. A

**40**, 1367 (1989).
[8] N. Konjevic and N. I. Uzelac, J. Quant. Spectrosc. Radiat. Transfer **44**, 61 (1990).
[9] D. Bertuccelli, G. Bertuccelli, and H. O. Di Rocco, Phys. Scr. **43**, 469 (1991).
[10] C. Pérez, I. de la Rosa, A. M. de Frutos, and S. Mar, Phys. Rev. A **44**, 6785 (1991).
[11] I. González, S. Mar, and V. Cardeñoso, Atti Fond. Giorgio Ronchi **41**, 501 (1986).
[12] I. de la Rosa, C. Pérez, A. M. de Frutos, and S. Mar, Phys. Rev. A **42**, 7389 (1990).
[13] Laura Devesa Fernández, Tesina de Licenciatura, Departamento de Física Aplicada III, Universidad de Valladolid, Valladolid, 1991 (unpublished).
[14] M. A. Gigosos and V. Cardeñoso, Report No. 181, Departamento de Optica, Universidad de Valladolid, Valladolid, 1992 (unpublished).
[15] R. Bayón, M. García, M. A. Gigosos, and S. Mar, Appl. Opt. (to be published).
[16] J. T. Davies and J. M. Vaughan, Astrophys. J. **4**, 1302 (1963).
[17] R. A. Alpher and D. R. White, in *Plasma Diagnostic Techniques*, edited by R. H. Huddlestone and S. L. Leonard (Academic, New York, 1965).
[18] J. Reader, C. H. Corliss, W. L. Wiese, and G. A. Martin, *Wavelengths and Transition Probabilities for Atoms and Atomic Ions*, Natl. Bur. Stand. Ref. Data Ser., Natl. Bur. Stand. (U.S.) Circ. No. 68 (U.S. GPO, Washington, DC, 1980).
[19] S. Garpman and N. Spector, J. Opt. Soc. Am. **66**, 904 (1976).
[20] M. Miller, R. Roig, and R. D. Bengtson, Phys. Rev. A **8**, 480 (1973).
[21] H. R. Griem, *Spectral Line Broadening by Plasmas* (Academic, New York, 1974).
[22] M. A. Levchenko, Izv. Vyssh. Uchebn. Zaved. Fiz. **10**, 147 (1971).
[23] V. P. Samoilov, Yu. M. Smirnov, and G. S. Starikova, Opt. Spektrosk. **38**, 1222 (1975) [Opt. Spectrosc. **38**, 707 (1975)].
[24] V. P. Podbiralina, Yu. M. Smirnov, and N. V. Stegnova, Opt. Spectrosc. **34**, 467 (1973).